Phase Noise Can Induce Stochastic Resonance ?

Jong-Hoon Huh[1,2], Yoshimitsu Yano[2], and Naoto Miyagawa[2]

[1]*Department of Physics and Information Technology, Faculty of Computer Science and Systems Engineering, Kyushu Institute of Technology, Fukuoka 820-8502, Japan*

[2]*Division of Mechanical Information Science and Technology, Graduate School of Computer Science and Systems Engineering, Kyushu Institute of Technology, Fukuoka 820-8502, Japan*

We investigated stochastic resonance (SR) of ac-driven electroconvection (EC) in nematic liquid crystals by employing the phase noise of the ac field. The phase noise smoothly varies the threshold of EC, as the amplitude noise does it. Surprisingly, a kind of phase stochastic resonance (PSR) is discovered in appropriately colored phase noises; thus, it provides nonmonotonic behavior of the threshold in which a peak of the pattern amplitude of EC is found as a function of the phase noise intensity. The colored and white phase noises are discussed for understanding the PSR.

Noise-induced phenomena have been extensively investigated in various fields, in order to understand the role of noise [1-3]. Generally, considering the fluctuations of material and/or control parameters in natural and artificial systems, noise (as the origin of the fluctuations) should be removed or minimized for desirable treatments. However, since Benzi et al. discovered stochastic resonance (SR) [4], noise has been reconsidered as a factor of constructive roles in control of order-disorder and enhancement of the output of various systems [1-3]. In particular, the idea of the enhancement of the output using an optimal noise level (not too small and not too large) has triggered useful applications in neuroscience [5], biophysics [6], photonics [7], mechanics [8], and image processing [9]. The crucial point of these SR phenomena is that a desirable signal can be maximized by controlling noise levels. Contrarily, the minimization of the signal-noise ratio (SNR) was also found in nervous systems [10-14] and nonequilibrium dissipative systems [15]; by analogy with SR, the phenomenon has been called inverse stochastic resonance (ISR) [11-15]. Note that the aforementioned SR and ISR occur in the *amplitude* noise added to the deterministic signal. Recently, Chowdhury et al. discovered random *phase* deviation-induced SR in a nanoelectromechanical membrane system [16], which was named as *phase stochastic resonance* (PSR). In PSR, additional phase noise in a deterministic signal plays a crucial role in the enhancement of the output, instead of the amplitude noise in conventional SR and ISR.

In this study, we address ac-driven electroconvection (EC) in a nematic liquid crystal (NLC). In principle, EC can be induced by applying an ac electric field across a thin layer (typically, $d = 10-100$ μm). The basic mechanism of EC was well explained in the earlier studies by Carr [17] and Helfrich [18]. The director fluctuations of an NLC resulting from thermal noise can be reinforced by a material flow via the Coulomb force acting on space charges that are focused by the electric anisotropy of an NLC; when the Coulomb force overcomes the viscoelastic and dielectric restoring forces at a critical threshold voltage V_c, electrohydrodynamic instability arises in the NLC layer; it provides a regular roll-pattern EC [i.e., so-called Williams domain (WD)] [19,20]. Our question is that how a weak signal below the threshold voltage can induce EC under additional phase noise in the signal.

In this Letter, we present an unexpected PSR found in EC by controlling phase noise; the evolution of EC patterns and

the threshold of EC are examined as a function of a random phase deviation of noise. The reader will find that the PSR appears only in *colored noise* adjusted appropriately (e.g., through low-pass filters of noise generators).

A typical NLC [*p*-methoxybenzylidene-*p*'-*n*-butylaniline (MBBA)] was used in this study; the planarly-aligned NLC sandwiched between two parallel transparent electrodes (indium tin oxide) was characterized by a conductivity of $\sigma_\perp$ = $2.01 \times 10^{-8}\ \Omega^{-1}\mathrm{m}^{-1}$ and a dielectric constant of $\varepsilon_\perp$ = 5.14 (at T = 25 ℃). Here, $\perp$ denotes the orientation perpendicular to the initial director $\boldsymbol{n}_0$ of the NLC [$\boldsymbol{n}_0$ = (1,0,0)]. The ac voltage $V(t)$ was applied across the thin slab of the NLC having a thickness d = 50 μm and a lateral (active) size $L_x \times L_y$ = 1 × 1 cm:

$$V(t) = V_0 \cos\{\omega_0 t + \phi_{N0}\xi(t)\} + A_{N0}\xi(t)\,, \qquad (1)$$

where A_{N0} indicates the noise intensity for the amplitude deviation of V_0 (A_{N0} = 0 in this study). For the phase deviation, a Gaussian-type noise [$-1 < \xi(t) < 1$] was externally introduced into a wave generator (WF1974, NF); ϕ_{N0} indicates the magnitude of the random phase deviation, which is a main control parameter in this study ($0 \leqq \phi_{N0} \leqq \pi$). Colored noises $\xi(t)$ characterized by the autocorrelation time τ_N [= $1/(2\pi f_c)$] as well as white noise ($\tau_N \to 0$: $f_c \to \infty$) were used; the cutoff frequency f_c of the noise was controlled by the low-pass filters of a synthesizer (7075, Hioki) [15]. The standard shadowgraph method for EC was used for optical observations and measurements [20]; the EC patterns and their dynamics were observed in the *xy* plane by using a computer-controlled image software system (Scion Image) and an image-capture board (Scion Corp., PCI-VE5) together with a charge-coupled device camera (Sony, XC-75) mounted on a polarizing microscope (Meijitech, ML9300). All measurements were performed at a fixed temperature of T = 25 ℃ by using an electrothermal control system (TH-99, Japan Hightech) [15].

First, to see the role of the phase noise to EC, the evolution of EC patterns was observed by increasing ϕ_{N0}, as shown in Fig. 1. For fixed values of the ac frequency f_0 = 2 kHz and ac voltage V (= V_{rms}) = 35.6 V (V_0 = 50.3 V) slightly below V_c = 37. 3 V, a rest state is set at ϕ_{N0} = 0 [Fig. 1(a)]. By increasing ϕ_{N0}, the rest state evolves into a typical WD at ϕ_{N0} = 0.873 rad [Fig. 1(b)], and then into a fluctuating WD (FWD) at ϕ_{N0} = 1.75 rad [Fig. 1(c)]. Certainly, owing to the phase noise ($\phi_{N0} \neq 0$), EC occurs in spite of a weak voltage below $V_c(\phi_{N0} = 0)$. Furthermore, the FWD reenters a normal WD at ϕ_{N0} = 2.41 rad, as shown in Fig. 1(d); then, it successively changes into the rest state at ϕ_{N0} = 2.62 rad [Fig. 1(e)]. This novel EC evolution driven by the phase noise has been first found in the present study. In general, a rest state (at $V < V_c$) successively evolves into a WD, an FWD, and a grid pattern, and then finally into a developed turbulent state with the increase of V_0 (A_{N0} = 0 and ϕ_{N0} = 0) [21], or with the increase of colored amplitude noise A_{N0} (ϕ_{N0} = 0 and a fixed V_0) [22]; furthermore, the reverse evolution is found with the decrease of V_0 [21,23], or with the increase of white amplitude noise A_{N0} (ϕ_{N0} = 0 and a fixed V_0) [22]. As displayed in the right column of Fig. 1, $V(t)$ applied to each pattern in the left column is modulated by the magnitude of ϕ_{N0}. Note that the optimal phase noise for the most developed EC state [e.g., Fig. 1(c)] exits, and the same rest state [i.e., Fig. 1(a) and 1(e)] or similar WDs [i.e., Fig. 1(b) and 1(d)] appear despite different $V(t)$ modulated by different phase deviations (with a same value of V_{rms}). Most importantly of all, this result was obtained by using a colored noise $\xi(t)$ having an appropriate cutoff frequency (e.g., f_c = 2 kHz in this study).

Next, to elucidate the evolution of EC mentioned above, we measured the threshold V_c of EC as a function of ϕ_{N0} (Fig. 2) by using the colored noise (f_c = 2 kHz); additionally, different f_c-noises $\xi(t)$ including white noise ($f_c \to \infty$) were also tested. Obviously, the colored phase noise (f_c = 2 kHz) causes nonmonotonic behavior of V_c; there exists a minimal V_c at $\phi_{N0}^{*} \sim 1.75$ rad. Accordingly, for the colored noise (f_c = 2 kHz), the WD and FWD [Figs. 1(b)-1(d)] were able to be observed at appropriate values of ϕ_{N0} ($0.7 < \phi_{N0} < 2.45$ rad) in spite of the application of low V [$< V_c(\phi_{N0} = 0) = 37.3$ V]; furthermore,

a rest state was found for $\phi_{N0} < 0.7$ rad [Fig. 1(a)] and also for $\phi_{N0} > 2.45$ rad [Fig. 1(e)]. On the other hand, the white phase noise monotonically increases V_c, whereas an extremely colored noise ($f_c = 500$ Hz), for which high frequencies (> 500 Hz) is filtered out, monotonically decreases V_c. Therefore, by increasing ϕ_{N0}, the white noise and the extremely colored noise provide the conventional pattern evolutions; e.g., no reentrance of the WD or rest state is found.

To understand this unusual phenomenon, we examined the power spectra of the voltages $V(\phi_{N0})$ modulated by the colored noise ($f_c = 2$ kHz); Fig. 3(a) shows those of the voltages $V(t)$ displayed in Fig. 1. By increasing ϕ_{N0}, the Fourier frequency components concentrated around the carrier frequency f_0 (at $\phi_{N0} = 0$) become gradually scattered with generating lower and higher frequency ones. The studies of EC under the combined ac fields [24] show that the voltages contribute to destabilizing or stabilizing EC, depending on frequencies lower or higher than a characteristic frequency f_{cd} (~ 2.3 kHz in this study) dividing the conduction and dielectric regimes for EC [20]. Accordingly, in the case of the colored phase noise, the additional low frequency effect may be dominant for small ϕ_{N0} ($< \phi_{N0}^*$), resulting in the decrease of V_c; contrastively, the additional high frequency effect may be dominant for large ϕ_{N0} ($> \phi_{N0}^*$), yielding the increase of V_c. These competitive effects may determine V_c (Fig. 2) as well as EC states (Fig. 1). Furthermore, the two effects are more clearly revealed in Fig. 3(b); the power sums, $\Sigma P(f < f_{cd})$ and $\Sigma P(f > f_{cd})$, indicate the destabilization and stabilization effects on EC, respectively; the former shows nonmonotonic behavior responsible for the unusual pattern evolution (Fig. 1 and Fig. 2), although ϕ_{N0}^* is slightly larger than that in Fig. 2. On the other hand, the white noise ($f_c \rightarrow \infty$) and extremely colored noise ($f_c = 500$ Hz) showed, respectively, high frequency-dominant effect and low frequency-dominant one for all ranges of ϕ_{N0}; e.g., at a fixed $\phi_{N0} = 1.75$ rad, compare with one another in the voltages and their power spectra having different f_c (Fig. 4). As a result, the white noise and extremely colored noises give rise to the monotonic increase and decrease of V_c, respectively (Fig. 2). Therefore, the reason why the different states occur for different f_c (Fig. 2) can be deduced: e.g., at fixed values of $\phi_{N0} = 2.41$ rad and $V = 37.3$ V [i.e, (d) in Fig. 2], a rest state ($V << V_c$) for white ($f_c \rightarrow \infty$), a WD ($V \approx V_c$) for $f_c = 2$ kHz, and turbulence ($V >> V_c$) for $f_c = 500$ Hz. In other words, the appropriately colored noise ($f_c = 2$ kHz) can give an optimal phase deviation [Fig. 1(c)] from the original phase $\omega_0 t$ of the carrier signal [Fig. 1(a)] for developing EC. This nonmonotonic behavior of $V_c(\phi_{N0})$ is similar to the threshold variation in the amplitude noise-induced $V_c(A_{N0})$ [15,22]; however, the underlain mechanisms are completely different from each other.

Owing to the contribution of high frequencies, chevron patterns characterized for high frequencies around f_{cd} were observed at V_c, instead of WDs [20,24,25]: e.g., $\phi_{N0} > 2.7$ rad for the colored noise $f_c = 2$ kHz and $\phi_{N0} > 1.8$ rad for the white noise; furthermore, owing to the contribution of low frequencies, breathing WDs often found at low frequencies (< 10 Hz) [24] were observed for the extremely colored noise ($f_c = 500$ Hz): e.g., $\phi_{N0} = 2.25$ rad; moreover, more complicated patterns such as defect lattices [26] appeared by the phase noise, which have not been understood in the standard EC theory [17-20].

In addition, to evaluate the phase noise-induced threshold shift as an SR phenomenon, the pattern amplitude of EC was measured as a function of ϕ_{N0}; a space-time map (STM) [Fig. 5(a)] was constructed by successively placing a one dimensional fixed line (X) arbitrarily selected in two dimensional images [e.g., Fig. 1(b)] with an identical time interval ($\Delta t = 1$ s in this study). Under the same conditions for Fig. 1 ($f_0 = 2$ kHz and $V = 35.6$ V), the present STM was obtained by a successively steplike increase and decrease of ϕ_{N0} ($\Delta\phi_{N0} = 0.174$ rad for every 10 s), as shown in Fig. 5(a); the one dimensional lines were placed for 10 s at every ϕ_{N0}. By increasing ϕ_{N0} from 0 to π, a pattern evolution appears: a rest state → WD → FWD → WD → a rest state; furthermore, by decreasing ϕ_{N0} from π to 0, the same pattern evolution is observed. Accordingly, Fig. 5(b) shows the variation of the pattern amplitude I of EC as a function of ϕ_{N0}; the normalized intensity I corresponds to the SNR. In Fig. 5(b), one finds a kind of SR (showing a peak of I) with respect to a deterministic signal-induced EC that cannot be induced by the weak intensity of the signal (i.e., below V_c); the difference of the magnitude

of I between increasing and decreasing ϕ_{N0} depends on the detail of EC [e.g., the optical intensity fluctuation resulting from motion of defects in Fig. 5(a); and see also Fig. 1(c)].

Finally, we have checked the present PSR by simulating the one dimensional Carr-Helfrich equations for EC [17,18,20]:

$$\dot{q} + \frac{q}{\tau} + \sigma_H \frac{V(t)}{d}\psi = 0, \tag{2}$$

$$\dot{\psi} + \lambda\left[E_0^2 + \left(\frac{V(t)}{d}\right)^2\right]\psi + \frac{q}{\eta}\frac{V(t)}{d} = 0. \tag{3}$$

Here, q and ψ denote, respectively, the space-charge density and the curvature of the director ($\psi = \partial\varphi/\partial x$) for the angle φ of the director deviation from the x axis (i.e., $\varphi = 0$ for $\boldsymbol{n}_0$); all parameters τ, σ_H, λ, η, and E_0 are determined by the detail of the NLC (MBBA in this study). In the numerical simulation of Eqs. (2) and (3) for the linear stability analysis [27], the nonmonotonic threshold behavior is successfully reproduced as a function of ϕ_{N0} (f_c = 2 kHz), as shown in Fig. 5(c).

In conclusion, a kind of PSR has been discovered in the EC system by employing *appropriately colored phase* noise; thus, it provides nonmonotonic behavior of the threshold of EC. The white phase noise and extremely colored phase noise cause monotonic increase and decrease of the threshold of EC, respectively. In the present PSR, the bell-shaped behavior of the EC pattern amplitude (resulting from the reversed bell-shaped threshold of EC) is found as a function of the phase-noise deviation; this result is originated from appropriate Fourier frequency components generated by the phase noise. In the EC system, competition between destabilization and stabilization effects on EC play a role in the PSR; the former effect occurs through the lower frequencies of noise spectra than a characteristic frequency for EC dividing conduction and dielectric regimes, whereas the latter one does through higher frequencies. The reciprocal effects can be controlled by the phase-noise deviation, and they can induce EC in spite of weak voltages below the threshold one; in particular, note that in colored phase noise adjusted appropriately with respect to the detail of EC, the PSR can be found.

PSR reported in the recent research [16] and the present study may enable various applications such as signal transmission and order-disorder control [3] together with SR [4-9] and ISR [10-15]; furthermore, the mixed phase-amplitude deviations [$A_{N0} \neq 0$ and $\phi_{N0} \neq 0$ in Eq. (1)] of signals are also expected in future research [16].

ACKNOWLEDGMENT

This study was supported by JSPS KAKENHI (No. 15K05215).

REFERENCES

1) W. Horsthemke and R. Lefever, *Noise-Induced Transitions* (Springer-Verlag, Berlin, 1984).

2) J. Garcia-Ojalvo and J. M. Sancho, *Noise in Spatially Extended Systems* (Springer-Verlag, New York, 1999).

3) F. Sagués, J. M. Sancho, and J. García-Ojalvo, Rev. Mod. Phys. **79**, 829 (2007).

4) R. Benzi, A. Sutera, and A. Vulpiani, J. Phys. A **14**, L453 (1981); C. Nicolis, *Tellus* **34**, 1 (1982); R. Benzi, J. Stat. Mech. P01052 (2009).

5) J. K. Douglass, L. Wilkens, E. Pantazelou, and F. Moss,
Nature (London) **365**, 337 (1993); S. M. Bezrukov and I. Vodyanoy, Nature (London) **378**, 362 (1995).

6) K. Wiesenfeld and F. Moss, Nature (London) **373**, 33 (1995).

7) B. McNamara, K. Wiesenfeld, and R. Roy, Phys. Rev. Lett. **60**, 2626 (1988); S. Barbay, G. Giacomelli, and F. Marin, Phys. Rev. E **61**, 157 (2000).
8) R. L. Badzey and P. Mohanty, Nature (London) **437**, 995 (2005); F. Mueller, S. Heugel, and L. J. Wang, Phys. Rev. A **79**, 031804 (2009).
9) A. Delahaies, D. Rousseau, J. –B. Fasquel, and F. Chapeau-Blondeau, J. Opt. Soc. Am. A **29**, 1211-1216 (2012) .
10) L. S. Borkowski, Phys. Rev. E **82**, 041909 (2010).
11) B. Gutkin, J. Jost, and H. C. Tuckwell, Naturwissenschaften, 96, 1091 (2009); H. C. Tuckwell and J. Jost, Phys. Rev. E **80**, 031907 (2009); Physica A, **391**, 5311 (2012).
12) D. Guo, Cogn. Neurodyn. **5**, 293 (2011).
13) M. Uzuntarla, Phys. Lett. A, **377**, 2585 (2013); M. Uzuntarla, J. R. Cressman, M. Ozer, and E. Barreto, Phys. Rev. E **88**, 042712 (2013).
14) D. Li, X. Cui, and Y. Yang, Neurocomputing **287**, 52 (2018).
15) J. -H. Huh, Phys. Rev. E **94**, 052702 (2016).
16) A. Chowdhury, S. Barbay, M. G. Clerc, I. Robert-Philip, and R. Braive, Phys. Rev. Lett. **119**, 234101 (2017).
17) E. F. Carr, Mol. Cryst. Liq. Cryst. **7**, 253 (1969).
18) W. Helfrich, J. Chem. Phys. **51**, 4092 (1969).
19) R. Williams, J. Chem. Phys. **39**, 384 (1963).
20) L. M. Blinov, *Electro-optical and Magneto-optical Properties of Liquid Crystals* [The Universities Press (Belfast) Ltd., Northern Ireland, 1983].
21) S. Kai and K. Hirakawa, Prog. Theor. Phys. Suppl. **64**, 212 (1978).
22) J. -H. Huh, Phys. Rev. E **84**, 025302(R) (2011); J. -H. Huh and S. Kai, J. Phys. Soc. Jpn. Lett. **77**, 063601 (2014).
23) J. -H. Huh, J. Phys. Soc. Jpn. **85**, 024002 (2016).
24) N. Eber, P. Salamon, and A. Buka, Liq. Cryst. Rev. **4**, 101 (2016).
25) J. -H. Huh, Y. Hidaka, A. G. Rossberg, and S. Kai, Phys. Rev. E **61**, 2769 (2000); J. -H. Huh, A. Kuribayashi, and S. Kai, Phys. Rev. E **80**, 066304 (2009).
26) N. Oikawa, Y. Hidaka, and S. Kai, Phys. Rev. E **70**, 066204 (2004).
27) V_c was obtained by automatic determination of $\psi(t) = \psi_0 \exp(\alpha t)$ first going to have a positive growth rate ($\alpha > 0$) through steplike increase of V with $\Delta V = 0.1$ V; i.e., the transition point from the relaxation to the rise of the director.

Figure Captions

FIG. 1. (Color online) Evolution of EC patterns in the smooth increase of the phase deviation ϕ_{N0} (at fixed values of V_0 = 50.3 V and f_0 = 2 kHz); left column: optical EC patterns for ϕ_{N0} = 0 (a), 0.873 (b), 1.75 (c), 2.41 (d), and 2.62 rad (e); right column: applied $V(t)$ for each corresponding EC pattern. A colored noise (f_c = 2 kHz) was used for the random phase deviation $\phi_N = \phi_{N0}\xi(t)$. See also Fig. 2.

FIG. 2. (Color online) Threshold voltage V_c of EC as a function of the phase deviation ϕ_{N0} of colored (f_c = 500 Hz and 2 kHz) and white ($f_c \rightarrow \infty$) noises. The thick arrow indicates increasing ϕ_{N0} (at a fixed V = 35.6 V < V_c = 37.3 V) for the evolution of EC, and (a)-(e) represent (ϕ_{N0}, V) for corresponding patterns in displayed in Fig. 1.

FIG. 3. (Color online) (a) Power spectra of $V(t)$ modulated by a phase noise (f_c = 2 kHz) at fixed values of V_0 = 50.3 V and f_0 = 2 kHz for various phase deviations ϕ_{N0}, (b) Power sums $\Sigma P(f < f_{cd})$ for the destabilization effect on EC and $\Sigma P(f > f_{cd})$ for the stabilization one (f_{cd} = 2300 Hz). The solid lines in (b) are a guide for the eye.

FIG. 4. (a) Applied voltages $V(t)$ modulated by ϕ_{N0} = 1.75 rad (at an identical V_0 = 50.3 V) for the noise cutoff frequencies f_c = ∞ (white noise), 2 kHz, and 500 Hz, (b) Power spectra of the corresponding $V(t)$; note the change of Fourier components around the carrier frequency f_0 = 2 kHz. These three kinds of $V(t)$ induce a rest state [Fig. 1(a)], an FWD [Fig. 1(c)], and a turbulent state, respectively.

FIG. 5. (Color online) (a) Space-time map (STM) for the EC-pattern evolution and (b) optical pattern intensity $I(\phi_{N0})$ with increasing and decreasing ϕ_{N0} (at fixed values of V_0 = 50.3 V and f_0 = 2 kHz); the STM optically observed was transformed into a normalized intensity I indicating the pattern amplitude of EC after averaging in X and a smoothing process of $I(t)$. (c) Calculated threshold voltage V_c as a function of ϕ_{N0}. For simulating Eqs. (2) and (3), the MATLAB R2018b was used with the Runge-Kutta method; V_c was determined at a colored noise (f_c = 2 kHz) provided by a frequency filtering program; compare it with the experimental one provided in Fig.2.

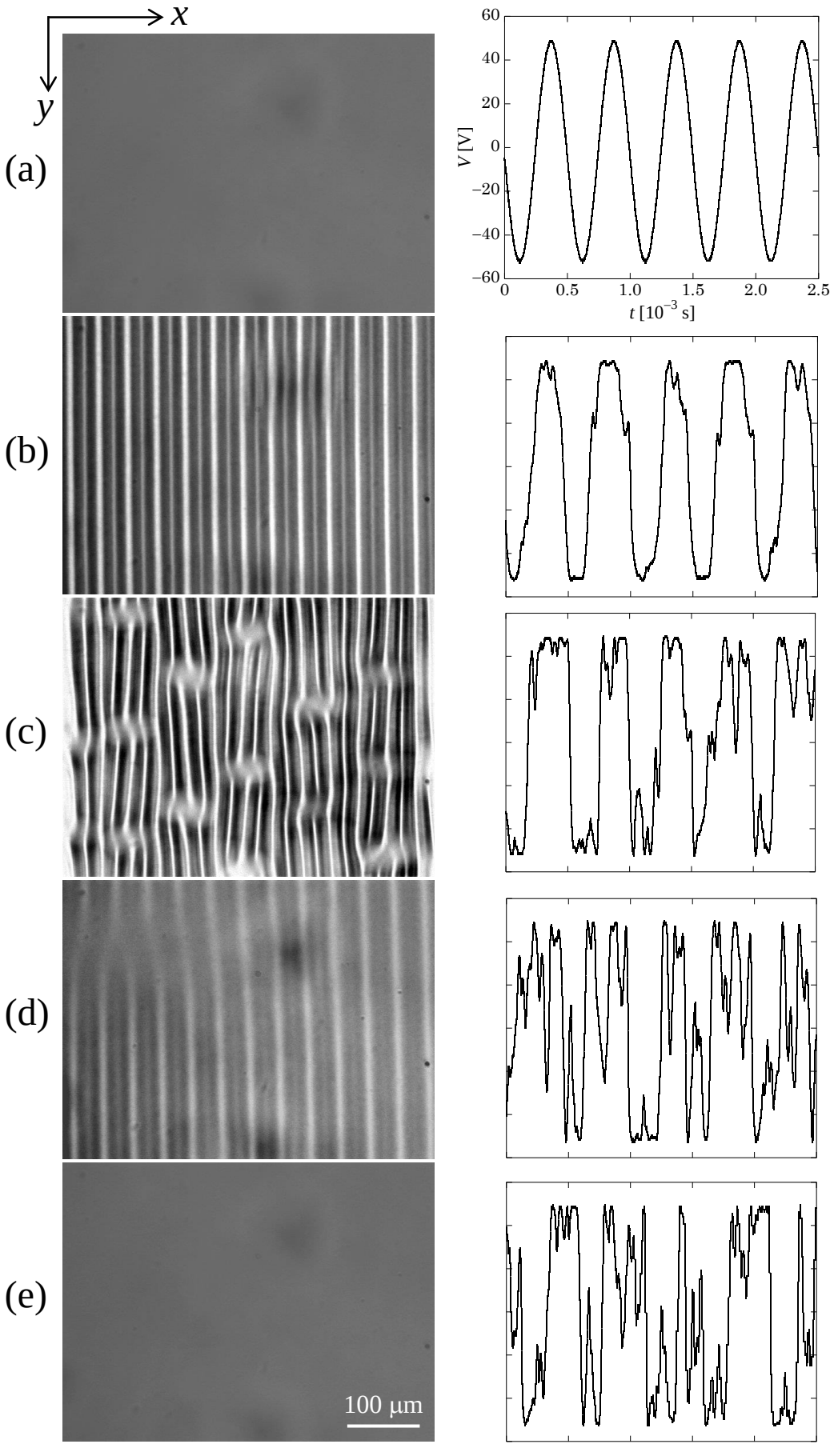

Fig. 1

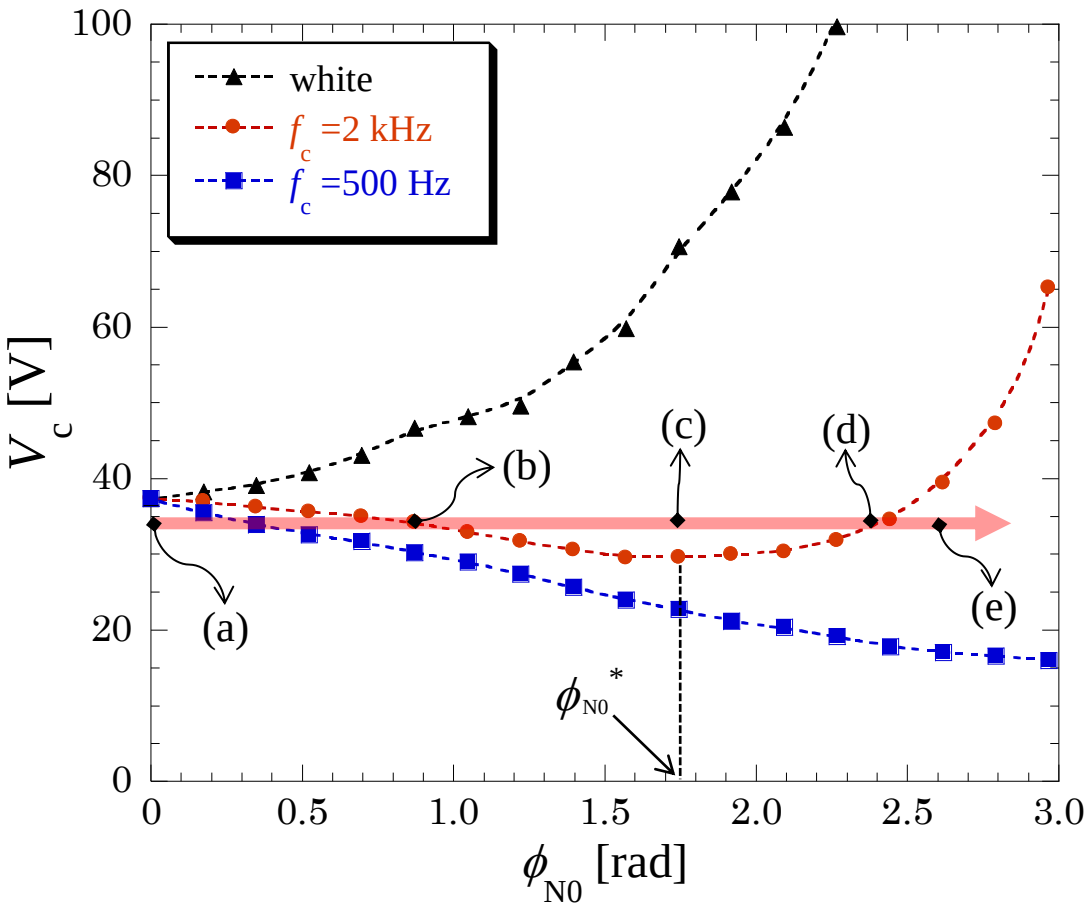
white
f_c =2 kHz
f_c =500 Hz
V_c [V]
ϕ_{N0} [rad]
ϕ_{N0}^*
(a)
(b)
(c)
(d)
(e)
0
20
40
60
80
100
0
0.5
1.0
1.5
2.0
2.5
3.0

Fig. 2

(a)

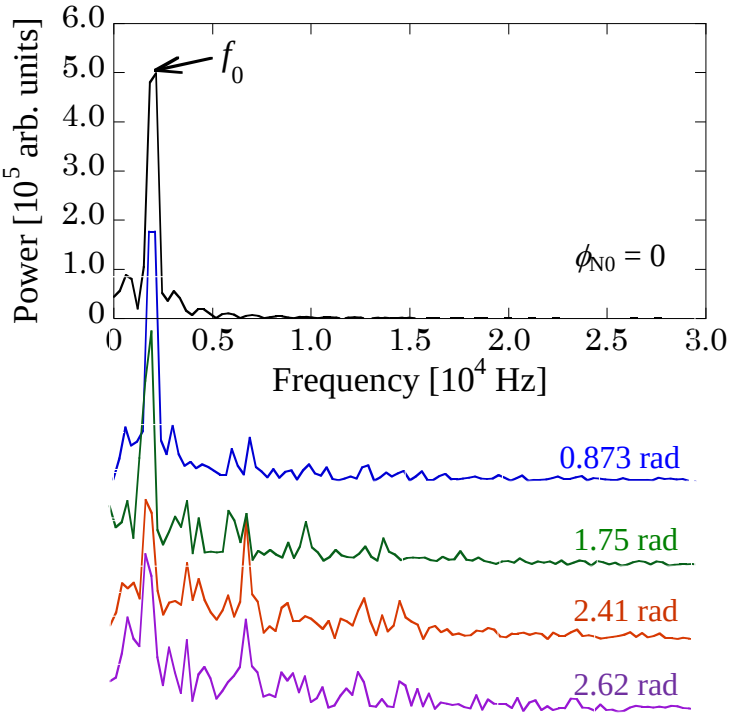
Power [10^5 arb. units]
6.0
5.0
4.0
3.0
2.0
1.0
0
f_0
ϕ_{N0} = 0
0
0.5
1.0
1.5
2.0
2.5
3.0
Frequency [10^4 Hz]
0.873 rad
1.75 rad
2.41 rad
2.62 rad

(b)

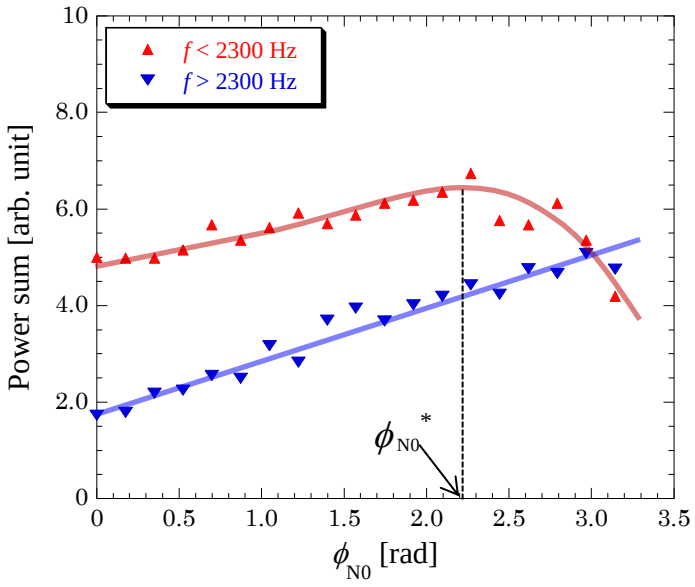
Power sum [arb. unit]
10
8.0
6.0
4.0
2.0
0
f < 2300 Hz
f > 2300 Hz
ϕ_{N0}^*
0
0.5
1.0
1.5
2.0
2.5
3.0
3.5
ϕ_{N0} [rad]

Fig. 3

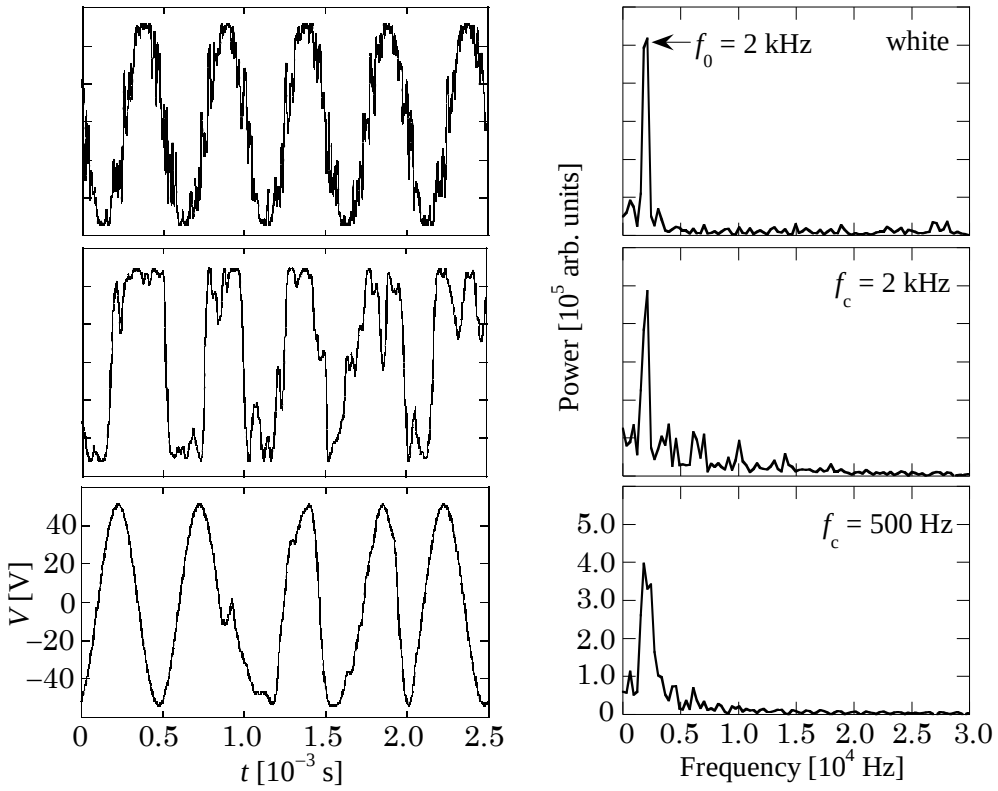
V [V]
40
20
0
−20
−40
0
0.5
1.0
1.5
2.0
2.5
t [10^−3 s]
(a)
f0 = 2 kHz
white
fc = 2 kHz
fc = 500 Hz
Power [10^5 arb. units]
5.0
4.0
3.0
2.0
1.0
0
0
0.5
1.0
1.5
2.0
2.5
3.0
Frequency [10^4 Hz]
(b)

Fig. 4

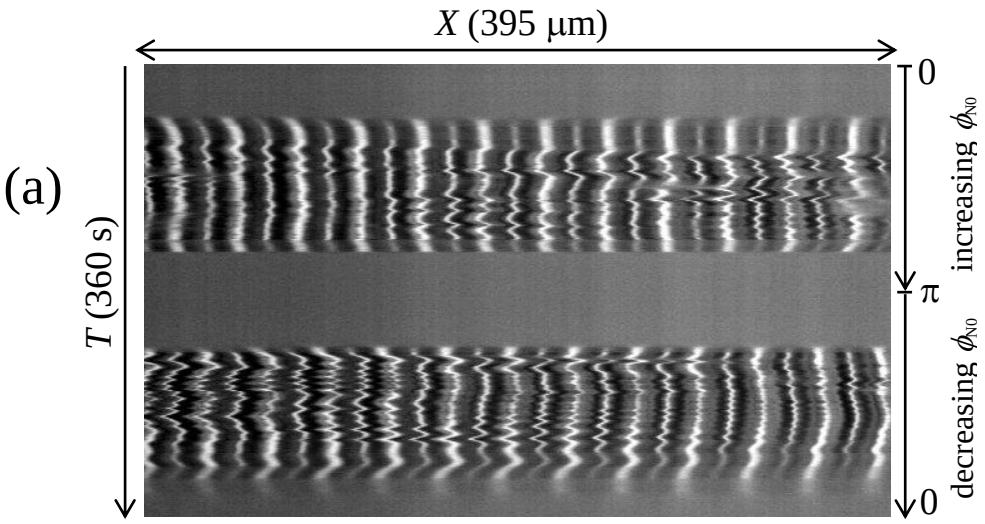
(a)
X (395 μm)
T (360 s)
0
π
0
increasing ϕ_{N0}
decreasing ϕ_{N0}

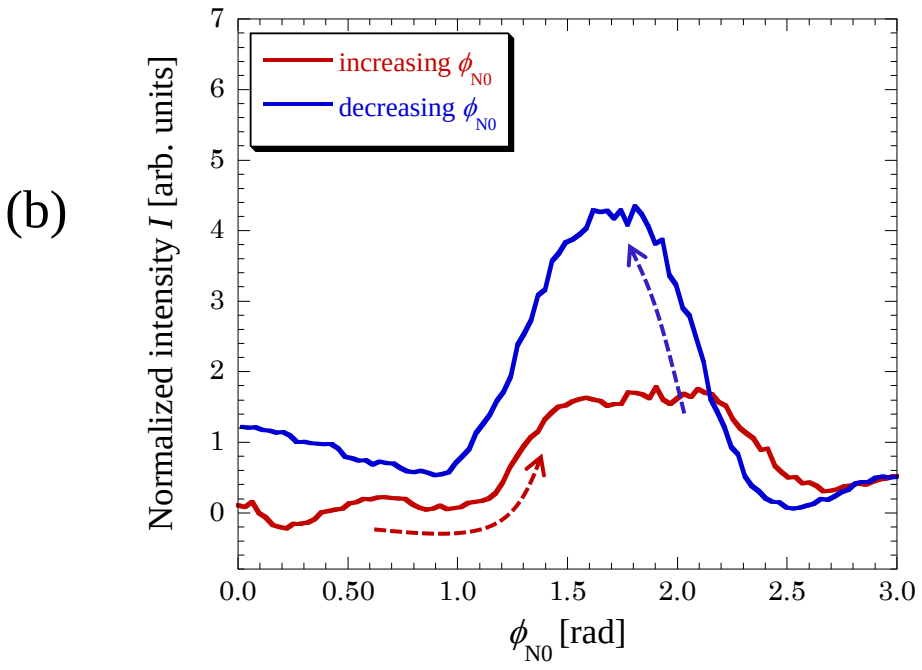
(b)
increasing ϕ_{N0}
decreasing ϕ_{N0}
Normalized intensity I [arb. units]
ϕ_{N0} [rad]

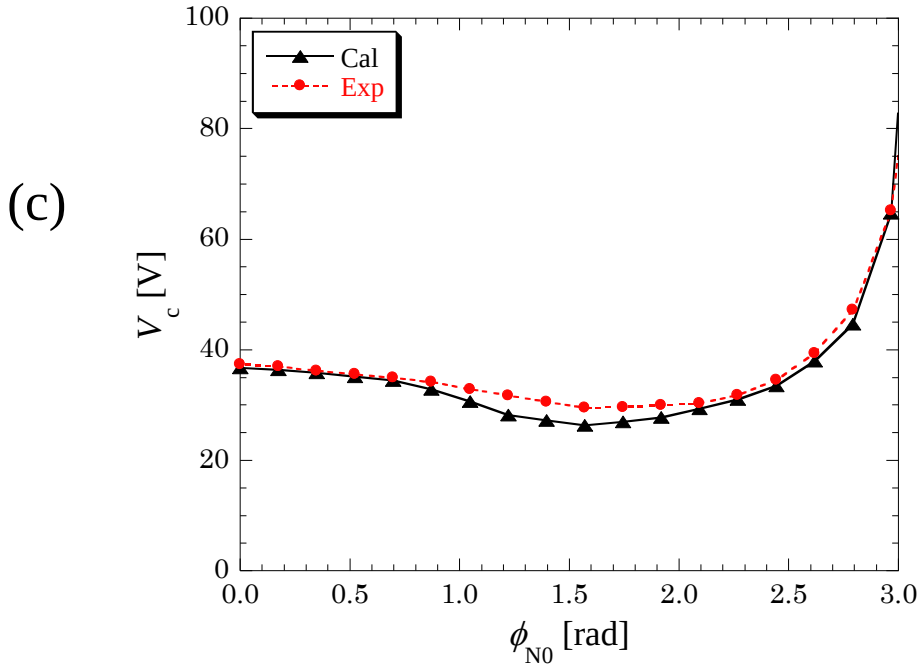
(c)
Cal
Exp
V_c [V]
ϕ_{N0} [rad]

Fig. 5